OXFORD

Journal of Geophysics and Engineering

Journal of Geophysics and Engineering (2022) **19**, 67–74 https://doi.org/10.1093/jge/gxab074

Pulse width research on half-sine excitation signal for bending vibrator

Kai Zhang[1,*], Fengbo Li[2], Jinping Wu[2], Baohai Tan[1] and Lei Liu[3]

[1] School of Geosciences and Technology, China University of Petroleum, Qingdao 266580, China
[2] Sinopec Research Institute of Petroleum Engineering, Beijing 102200, China
[3] Shengli Well Logging Co., Dongying 257055, China

*Corresponding author: Kai Zhang. E-mail: kai@upc.edu.cn

Received 10 October 2021, revised 4 November 2021
Accepted for publication 25 November 2021

Abstract

Acoustic well logging adopts bending vibrators to transform high-voltage electric signals into acoustic signals. Excited acoustic signals have been proven best when the pulse widths are $0.5/f_0$ (f_0 refers to the resonance frequencies of the bending vibrator). However, acoustic logging uses transformers to improve the excitation power, and these transformers change the rectangular excitation signals into similar half-sine signals. We study the relationships between the pulse widths of the similar half-sine excitation signals and the characteristics of the excited acoustic signals. Finite element analyses are performed to investigate the displacements of the center node on the surface of the piezoelectric ceramics that are excited by the pulse signals of different widths. Then, we design a circuit to realise the rectangular and half-sine excitation signals. Subsequently, acoustic experiments are carried out in our sound-deadening water tank to certify the simulation results. Results indicate that the best pulse width is $0.75/f_0$.

Keywords: bending vibrator, pulse width, excitation signal, acoustic logging, finite element simulation

1. Introduction

Acoustic well logging tools play an important role in detecting the lithology and porosity of underground formation that are used for oil and gas exploration and exploitation (Lu *et al.* 2014; Wang *et al.* 2015; Lu *et al.* 2017; Li *et al.* 2020). Among these tools, bending vibrators are adopted for transformations between electric energy and sonic energy (Zhang *et al.* 2017b). This kind of bending vibrator is composed of one rectangular tabular metal substrate holder and two pieces of rectangular tabular piezoelectric ceramics (figure 1). Piezoelectric ceramics are bonded on the two sides of the metal substrate holder, and the polarisation orientation is along the height orientation and parallel to the z-axis. The metal substrate holder is much longer than the piezoelectric ceramics, allowing the bending vibrator to be electrically connected and physically fixed. Excited by electronic pulses, the piezoelectric ceramic on one side undergoes extension, while the other side undergoes contraction. Thus, the bending vibrator obtains bending oscillation and emits acoustic waves.

During acoustic well logging, the power of the acoustic signal excited by the bending vibrators should be as large as possible to improve the detection range. Meanwhile, the 3-dB bandwidths should be as narrow as possible to realise the best signal-to-nose ratio (Zhang *et al.* 2021). These characteristics of the emitted sonic waves determine the working performance of the logging tools. Meanwhile, these characteristics are collectively determined by the bending vibrators and their excitation circuits. Thus, many studies have been conducted on the relationships between the operational performances of the bending vibrators and the pulse widths of their excitation signals (Bera *et al.* 2010; Svilainis *et al.* 2015; Deng *et al.* 2020; Onykiienko *et al.* 2020; Botero & Alunno

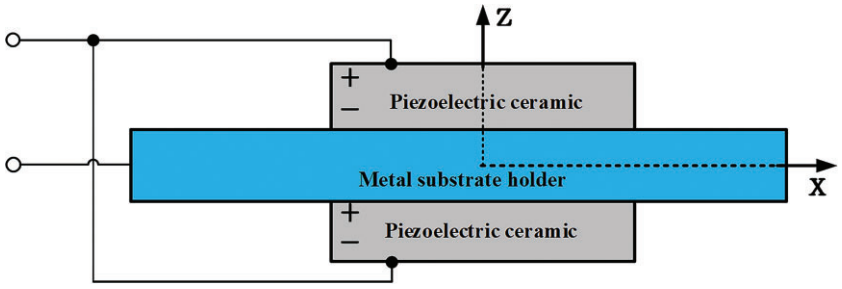

Figure 1. The bending vibrator used in acoustic logging is composed of one metal substrate holder and two pieces of piezoelectric ceramics.

2021). Most research is focused on rectangular pulse signals, and vibrators have been universally acknowledged to obtain the largest power when the pulse widths of their excitation signals are $0.5/f_0$ (f_0 refers to the resonance frequency of the bending vibrator) (Fa *et al.* 1996; Francek *et al.* 2019).

However, the excitation circuits of acoustic well logging tools usually use transformers to achieve a high voltage of thousand volts (Lu *et al.* 2017). These transformers that can be partly regarded as filters change the rectangular excitation signals into similar half-sine signals (Wang *et al.* 2017). Meanwhile, sine excitation signals have been researched and proven capable of obtaining excellent frequency characteristics (Tan *et al.* 2018). Unlike those of the rectangular signals, the relationships between the pulse widths of the similar half-sine excitation signals and the emitted acoustic signals have not been obtained. This research aims to study the relationships through simulations and experiments. In 2017, we introduced a high-voltage rectangular excitation method without transformers (Zhang *et al.* 2017a). In 2018, we designed a kind of excitation circuit to realise sinewave pulse signals on the basis of push–pull amplification technology (Tan *et al.* 2018). In this work, we first perform finite element analysis to obtain these relationships. Second, on the basis of aforementioned circuits, we design a circuit to realise the rectangular and half-sine vibrator excitation signals in the same circuit. Last, acoustic experiments are conducted in our sound-deadening water tank with the new excitation circuit.

2. Finite element simulation

Transient kinetic analysis was performed to obtain the transducer transient time and the frequency domain response characters (Kim & Kim 2009; Masmoudi *et al.* 2009; Narayanan & Schwartz 2010; Yaacob *et al.* 2011; Wu *et al.* 2012). Finite element analysis models were built in the ANSYS software. Three methods are usually adopted in transient kinetic analysis while executing the ANSYS software, namely, the full, reduced, and mode superposition methods. In this paper, the full method is used for the example analysis, while a sparse matrix solver is selected to obtain the solution. By analysing harmonic responses, the first order bending vibration can be excited along the length of the transducer, which is encouraged by the electronic signal of certain amplitude and frequency. Hence, the first mode bending vibration (hereafter referred to as the ground state) is studied in this paper. The material for the metal substrate holder was 45# steel whose length, width and thickness were 24, 9 and 1 mm, respectively. The material of the piezoelectric ceramic was PZT-8 whose length, width and thickness were 12, 9 and 1 mm, respectively. The density, Poisson ratio and Young's modulus of the metal substrate holder were 7800 kg/m^3, 0.28 and 21.6 × 1010 N/m^2, respectively. The essential parameters for the piezoelectric ceramic namely, the rigidity matrix [c], the piezoelectric coefficient matrix [e] and the dielectric coefficient matrix [ε], are expressed as follows:

$$[c] = \begin{bmatrix} 14.688 & 8.109 & 8.105 & & & \\ & 14.688 & 8.105 & & & \\ & & 13.171 & & & \\ & & & 3.289 & & \\ & & & & 3.135 & \\ & & & & & 3.135 \end{bmatrix} \times 10^{10} \frac{N}{m^2}, \quad (1)$$

$$[e] = \begin{bmatrix} 0 & 0 & -3.8754 \\ 0 & 0 & -3.8754 \\ 0 & 0 & 13.911 \\ 0 & 0 & 0 \\ 0 & 10.345 & 0 \\ 10.345 & 0 & 0 \end{bmatrix} {}^{N}/_{V \cdot m}, \quad (2)$$

$$[\varepsilon] = \varepsilon_0 \begin{bmatrix} 904.26 & & \\ & 904.26 & \\ & & 561.38 \end{bmatrix} = \begin{bmatrix} 7.99 & & \\ & 7.99 & \\ & & 4.96 \end{bmatrix} \times 10^{-9} \, {}^{C}/_{m}. \quad (3)$$

The time and frequency domain equations of the rectangular pulse signal whose duration and pulse width are

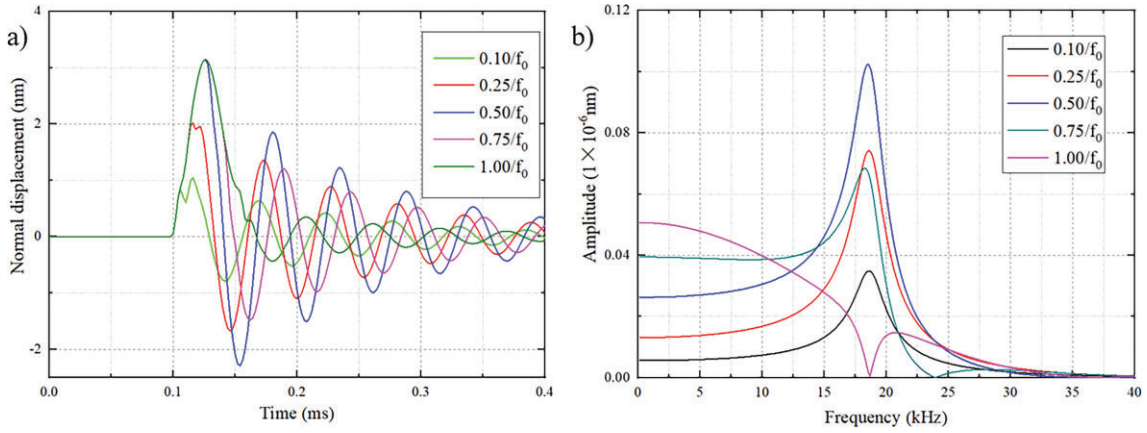

Figure 2. (a) The time-domain normal displacement comparison diagrams and (b) the corresponding spectral distribution comparison diagrams of the center node on the surface of the piezoelectric ceramics, which are excited by rectangular voltage signals of different widths.

denoted as t_0 and τ are as follows:

$$U(t) = \begin{cases} U_0 & (t_0 \le t \le t_0 + \tau) \\ 0 & (t\langle t_0, t\rangle t_0 + \tau) \end{cases}, \tag{4}$$

$$U(\omega) = e^{-j\omega t_0}\frac{U_0}{j\omega}\left(1 - e^{-j\omega\tau}\right), \tag{5}$$

where $U_0(1\text{V})$ is the amplitude of the excitation signal. The following pulse widths are selected: $0.1/f_0$, $0.25/f_0$, $0.5/f_0$, $0.75/f_0$, $1.0/f_0$ and $5.0/f_0$ (f_0 is the ground state resonance frequency of the bending vibrator and 18.2 kHz for the fixed-boundary air condition). Meanwhile, the bending vibrator was in the fixed-boundary condition. Therefore, displacement constraints ($U_X = 0$, $U_Y = 0$ and $U_Z = 0$) were added to the nodes of $X = \pm 9$ mm along the length of the metal substrate holder.

The time and frequency domain equations of the half-sine pulse signal are as follows:

$$U(t) = \begin{cases} U_0 \sin\frac{\pi(t-t_0)}{\tau} & (t_0 \le t \le t_0 + \tau) \\ 0 & (t\langle t_0, t\rangle t_0 + \tau) \end{cases}, \tag{6}$$

$$U(\omega) = e^{-j\omega t_0}\frac{U_0}{2j}\left[F\left(\omega - \frac{\pi}{\tau}\right) - F\left(\omega + \frac{\pi}{\tau}\right)\right], \tag{7}$$

$$\mathrm{F}(\omega) = \frac{1}{j\omega}\left(1 - e^{-j\omega\tau}\right), \tag{8}$$

where the duration, maximum voltage and pulse width of this signal are t_0, U_0 and τ, respectively. U_0 (1V) is the amplitude of the excitation signal. The following pulse widths were selected for the simulations: $0.1/f_0$, $0.25/f_0$, $0.5/f_0$, $0.75/f_0$ and $1.0/f_0$, where f_0 is the resonance frequency of the bending vibrator.

The time-domain normal displacement diagrams (a) and the corresponding spectral distribution diagrams (b) for the center node on the surface of the piezoelectric ceramics are shown in figure 2. The vibrator is excited by rectangular voltage signals of different widths. Thus, the normal displacement amplitude and the corresponding spectral amplitude are largest when the pulse width is $0.5/f_0$. Meanwhile, the wave obtains the narrowest 3-dB bandwidths because the subsequent waves come after the first wave peak excited by the rising edge and the subsequent waves excited by the falling edge are added by the same phase when their widths are $0.5/f_0$. In contrast, the two subsequent waves are added by different phases when their widths are not $0.5/f_0$. That is, the normal displacement amplitudes on the surface of the bending vibrators and the emitted energies are largest and the electromechanical conversion efficiencies are highest when the widths of the rectangular signals are $0.5/f_0$.

The time-domain normal displacement diagrams (figure 3a) and the corresponding spectral distribution diagrams (figure 3b) for the center node on the surface of the piezoelectric ceramics are shown in figure 3. The vibrator is excited by half-sine electric signals of different widths. Thus, the normal displacement amplitude and its corresponding spectral amplitude are the largest when the pulse width of the rectangular signal is $0.75/f_0$. Furthermore, the waves obtain the narrowest 3-dB bandwidths at this time. That is, the normal displacement amplitude on the surface of the bending vibrator and the emitted energy are the largest and the electromechanical conversion efficiencies are the highest when the width of the half-sine signals is $0.75/f_0$, unlike those of the rectangular voltage signals.

These figures show that the normal displacement amplitudes are the largest when the pulse widths are $0.5/f_0$ for the rectangular voltage signals and $0.75/f_0$ for the half-sine voltage signals. Figure 4 presents the time-domain normal displacement comparison diagrams (figure 4a) and the corresponding spectral distribution comparison diagrams (figure b) that are excited by the rectangular and half-sine voltage signals of the best widths. The normal displacement amplitudes and the corresponding spectral amplitudes of

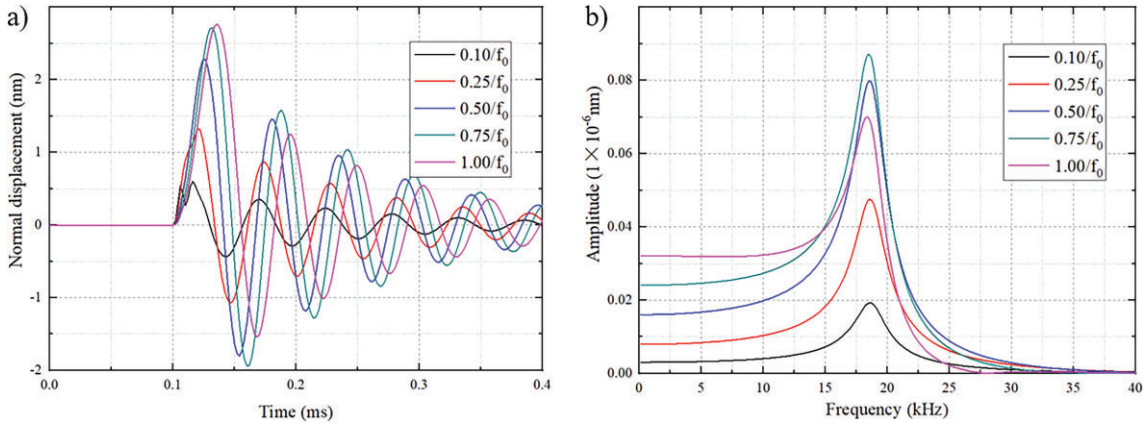

Figure 3. (a) The time-domain normal displacement comparison diagrams and (b) the corresponding spectral distribution comparison diagrams of the center node on the surface of the piezoelectric ceramics, which are excited by half-sine electric signals of different widths in the fixed-boundary condition.

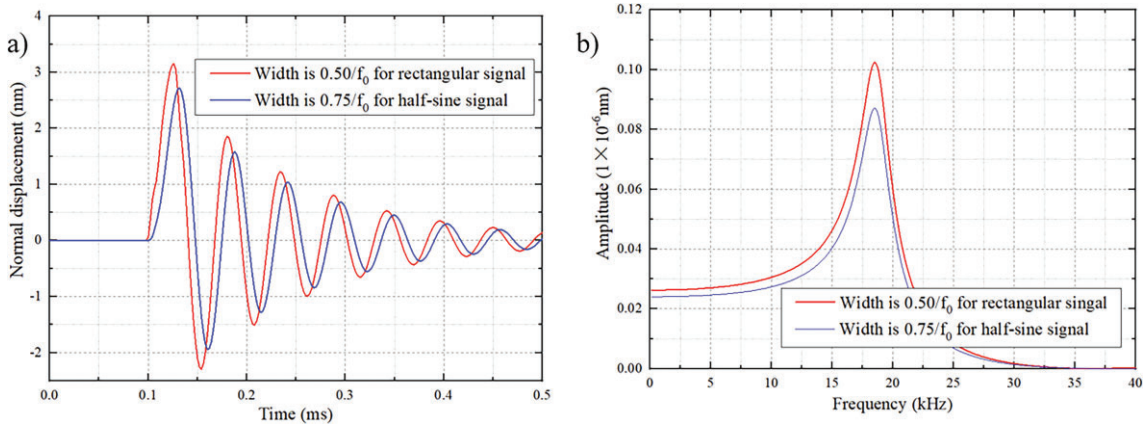

Figure 4. (a) The time-domain normal displacement comparison diagrams and (b) the corresponding spectral distribution comparison diagrams of the center node on the surface of the piezoelectric ceramics, which are excited in the fixed-boundary condition by the rectangular voltage signals whose width are $0.5/f_0$ and the half-sine voltage signals whose width are $0.75/f_0$.

the rectangular signals are larger than those of the half-sine signals because when all the other conditions are the same, the input power of the rectangular signals for the bending vibrators is the largest among the other signals. This conclusion is consistent with that of our earlier studies. In our earlier research, we found that the sound pressures of the acoustic signals emitted by rectangular excitation signals are much bigger than those of the acoustic signals emitted by the half-sine excitation signals, while other conditions remained unchanged (Zhang *et al.* 2017a).

3. Acoustic experiments

3.1. *Design of excitation circuit*

Acoustic experiments were designed to certify the simulation endings. To avoid irrelevant detrimental effects, the same bending vibrator was excited by the same circuit, producing the rectangular and half-sine signals of different widths. Thus, we designed a new excitation circuit to obtain rectangular and half-sine excitation signals for the bending vibrators. Figure 5 shows that the excitation circuit consisted of a transmitting controller, a signal generator, a rectifier circuit, a power amplifier, a high-voltage power supply circuits, a series of storage capacitors, a V-groove metal-oxide semiconductor (VMOSEFT) and its driver circuit. The transmitting controller was a DSP, a kind of high-speed digital signal processer. It collected control signals via the CAN bus, and these control signals were approximately about the amplitudes, the pulse widths and the phases of the excitation signals (Zhang *et al.* 2016). To obtain the half-sine signals, the DSP chip obtained the half-sine data stored in its FLASH storage (Zhang *et al.* 2014), and transferred these data into the signal generator to produce low voltage control signals. These control signals were adjusted by the rectifier circuit to change their amplitudes and frequencies. Thereafter, these signals were amplified by the power amplifier to improve their driving power and then by a transformer to thousands of volts. Last,

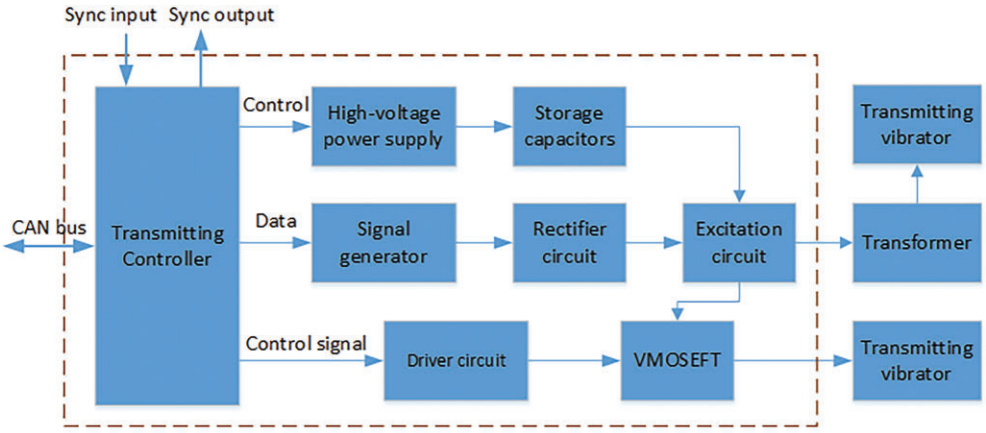

Figure 5. The structure diagram of the designed circuit, which can produce the rectangular and half-sine signals of different widths.

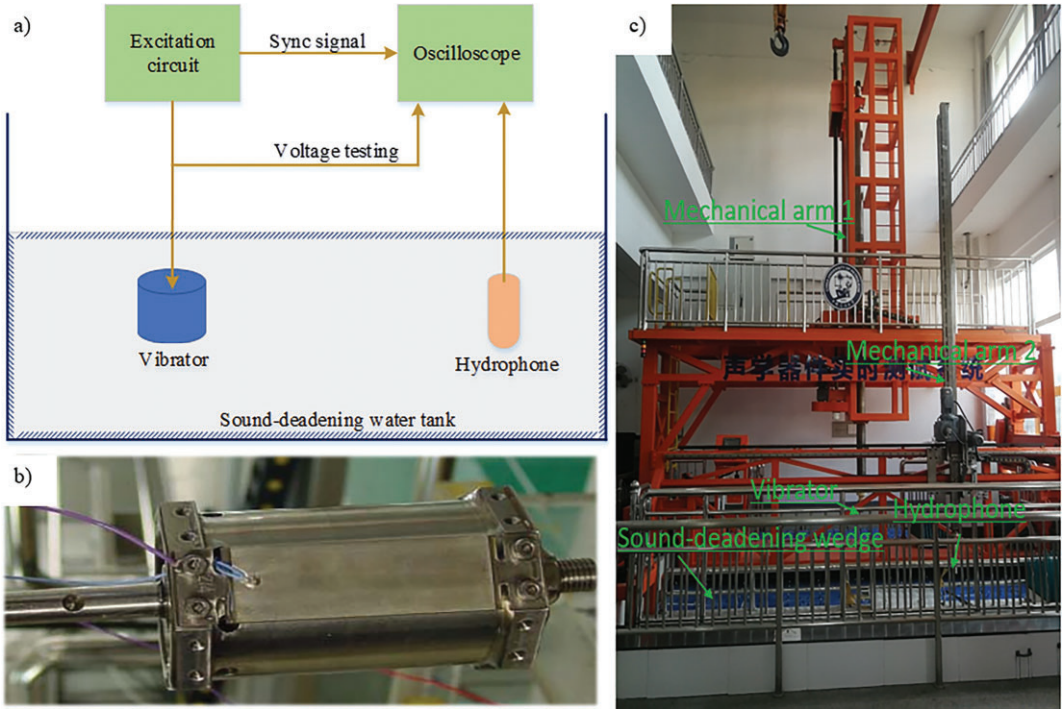

Figure 6. (a) The structure figure of acoustic waveform experimental system, (b) the diagrams of a fixed bending vibrator and (c) the positioning control system above the water tank.

high-voltage excitation signals were applied to the transmitting vibrator. To obtain the rectangular signals, the DSP produced control signals of intended widths and amplitudes, and delivered these signals to the high-speed VMOSFET driver circuit (IR2213). Afterward, the IR2213 chip triggered the VMOSFET chip to begin working, and the VMOSFET chip delivered electronic excitation signals from the high-voltage storage capacitors to the transmitting vibrator.

3.2. *Acoustic experiments in the sound-deadening water tank*

Acoustical experiments were carried out in our 6.0 × 6.0 × 6.0 m sound-deadening water tank (Zhang *et al.* 2021). The experiment system included the designed circuit, a fixed bending vibrator, a positioning control system, a broadband hydrophone and an oscilloscope (figure 6). The six planes of the water tank are filled with sound-deadening wedges (the blue materials), which can

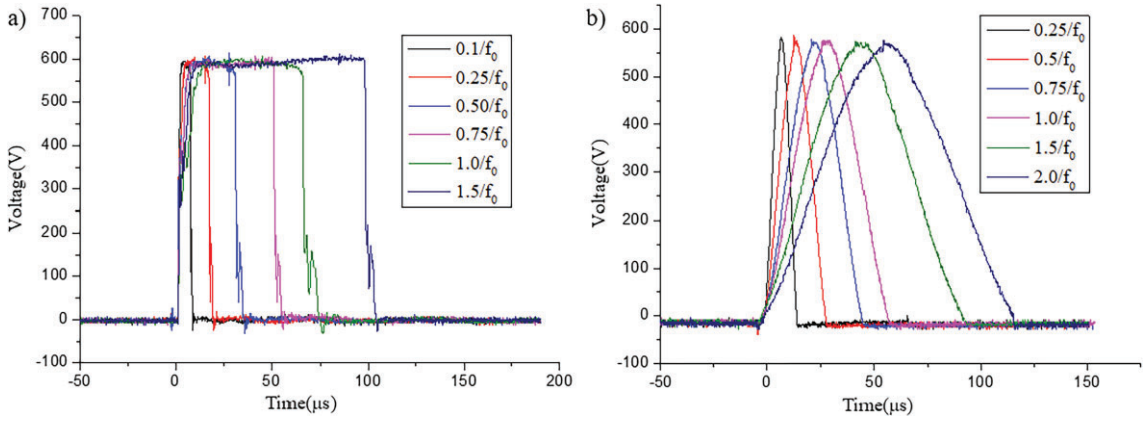

Figure 7. (a) The time-domain rectangular and (b) half-sinewave excitation signals of different widths excited by the excitation circuit.

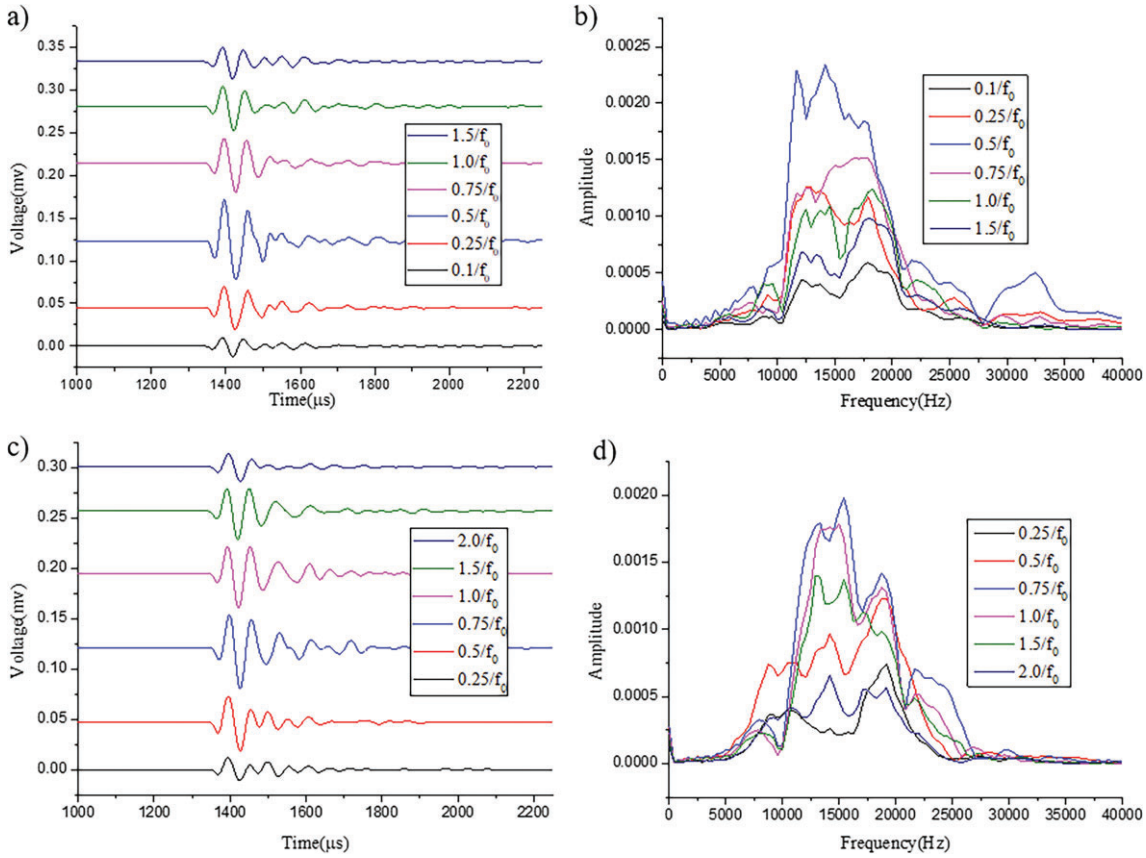

Figure 8. The (a, c) time-domain and (b, d) frequency domain acoustic waves excited by (a, b) rectangular and (c, d) half-sinewave excitation signals of different widths.

absorb more than 99% of acoustic signals. The vibrator is excited by the designed circuit and fixed on the first mechanical arm. This arm can realise precision position in three dimensions and circumferential space. The hydrophone is fixed on the second mechanical arm, which can only realise precision position in three dimensions. The material for the metal substrate holder of the vibrator was 45# steel whose length, width and thickness were 102, 25 and 1.6 mm, respectively. The material of the piezoelectric ceramic was PZT-8 whose length, width and thickness were 72, 25 and 1 mm, respectively. The boundary condition is a fixed-boundary silicon oil condition. The resonance frequencies of the bending vibrators were measured by an impedance analyser in advance, and the bending vibrator with a resonance frequency of 15.5 kHz was selected to be the transmitter. The hydrophone was accurately positioned by the positioning control system. According to the main workflow, the excitation circuit produced high-voltage electronic signals of different widths to

excite the transducer. Meanwhile, synchronising signals were sent out to start the concurrent data acquisition of the oscilloscope. Afterward, the acoustic waves emitted by electronic signals of different shapes and widths were transmitted via the water and finally received by the hydrophone. Figure 7 presents the time-domain rectangular and half-sinewave excitation signals of different widths excited by the excitation circuit, indicating that the excitation circuit obtained the required excitation signals.

4. Discussion and conclusions

Like previous theoretical research endings, the experiment endings in this study illustrate that the emitted acoustic energies are the largest and the 3 dB bandwidths are the narrowest when the widths of the rectangular excitation voltage signal are $0.5/f_0$ (f_0 refers to the resonance frequency of the bending vibrator). However, when transformers are adopted, the rectangular signals change to similar half-sine signals. The simulation and experimental results proved that the best pulse width is $0.75/f_0$ (figure 8). Bending vibrators perform free vibrations when excited by the rectangular signals. These vibrations consist of the vibrations caused by the rising edge of the excitation signals and the falling edge. When the two vibrating displacements obtain the same phases, the amplitudes of the excited waves are added together, producing the maximum amplitude. Bending vibrators obtain forced vibrations when excited by the half-sine signals. However, theoretical explanations have not been researched and reported.

This paper discusses the similar half-sine signals caused by transformers. However, half-sine and sinewave signals can also be achieved by other methods, producing consistent conclusions. Meanwhile, most of the complicated excitation signals can be regarded as the combination of rectangular and sinewave signals, and this study may be beneficial to these signals. Additionally, although this study focused on the bending vibrators of acoustic logging, it is of significance to transducers of other shapes and in other domains.

Considerable attention should be given to the impedance matching between the excitation circuit and the transmitting transducers in the acoustic experiments because poor impedance matching may lead to incorrect experiment endings.

Acknowledgements

This research is financially supported by Natural Science Youth Foundation of China (grant no. 41804121), Natural Science Foundation of China (grant no. 41774138), Major Scientific and Technological Projects of CNPC (grant no. ZD2019-183-004), and National Key R&D Program of China (grant no. 2019YFA0708301). The authors would like to express their gratitude to all the agencies for funding this research.

Conflict of interest statement: None declared.

References

Bera, S.C., Sarkar, R. & Mandal, N., 2010. Study of the effect of excitation frequency on electrode polarization impedance-type flow transducer, *IEEE Transactions on Instrumentation and Measurement,* **59**, 3289–3295.

Botero, A.Y. & Alunno, M., 2021. Signal modeling of the conditioning stage of a parametric array loudspeaker by statistical design of experiments, *Applied Acoustics*, **174**, https://doi.org/10.1016/j.apacoust.2020.107713.

Deng, Y., Zhang, G. & Zhang, X., 2020. A method to depress the transmitting voltage response fluctuation of a double excitation piezoelectric transducer, *Applied Acoustics,* **158**, https://doi.org/10.1016/j.apacoust.2019.107066.

Fa, L., Lin, H. & Chen, W.H., 1996. Transient character analyses for thin ring piezoelectronic transducers used in oil exploration, *Chinese Journal of Geophysics (in Chinese)*, **S1**, 387–399.

Francek, P., Petosic, A., Budimir, M. & Hrabar, I., 2019. Electrical resonance/antiresonance characterization of NDT transducer and possible optimization of impulse excitation signals width and their types, *NDT & E International,* **106**, 29–41.

Kim, J. & Kim, H.S., 2009. Finite element analysis of piezoelectric underwater transducers for acoustic characteristics, *Journal of Mechanical Science and Technology,* **23**, 452–460.

Li, S., Su, Y. & Tang, X., 2020. Research on a fast inversion method for structural strike around a borehole based on four-component dipole shear wave reflection imaging, *Chinese Journal of Geophysics,* **63**, 2478–2487 (in Chinese).

Lu, J., Ju, X., Men, B., Zhao, H., Qiao, W. & Duan, W., 2017. An acousto-electric effect logging detector in boreholes, *Journal of Geophysics and Engineering,* **14**, 397–407.

Lu, J.Q., Ju, X.D., Qiao, W.X., Men, B.Y., Wang, R.J. & Wu, J.P., 2014. Azimuthally acoustic logging tool to evaluate cementing quality, *Journal of Geophysics and Engineering*, **11**.

Masmoudi, M., Hosten, B. & Biateau, C., 2009, Analytical and finite element methods for studying the influence of the air-coupled transducer characteristics on the purity of guided waves generated in solids, in *36th Annual Review of Progress in Quantitative Nondestructive Evaluation*, University of Rhode Island, Kingston, RI, pp. 1061–1068.

Narayanan, M. & Schwartz, R.W., 2010. Design, fabrication and finite element modeling of a new wagon wheel flextensional transducer, *Journal of Electroceramics,* **24**, 205–213.

Onykiienko, Y., Batina, O., Vlasyuk, G., Shvaichenko, V., Mitsukova, A. & Marchenko, O., 2020. *The Selection of the Test Pulse Duration for a Shock Excitation Study of Ultrasonic Transducers*, 2020 IEEE 40th International Conference on Electronics and Nanotechnology (ELNANO), 499–502.

Svilainis, L., Dumbrava, V. & Chaziachmetovas, A., 2015. Investigation of the half bridge and transformer push-pull pulser topologies for ultrasonic transducer excitation, *Journal of Circuits Systems and Computers,* **24**.

Tan, B., Tang, X. & Zhang, K., 2018. Sine-wave pulse excitation circuit method and experiment study for LWD acoustic logging, *Well Logging Technology*, **42**, 629–633 (in Chinese).

Wang, C., Ning, Z., Zhang, K., Zuo, J., Zhang, B. & Chen, Y. 2017. *Analysis of Inductive Filtering Technology Based on Multi-winding Transformer and Its typical Practical Application*, IEEE Conference on Energy Internet and Energy System Integration (EI2), 2017, 1–6.

Wang, H., Tao, G. & Shang, X., 2015. A method to determine the strike of interface outside of borehole by monopole borehole acoustic reflections, *Journal of Petroleum Science and Engineering*, **133**.

Wu, J., Qiao, W. & Che, X., 2012. The finite element analysis of a piezoelectric bender used in acoustic logging, *Applied Acoustics (in Chinese)*, **31**, 86–92.

Yaacob, M.I.H., Arshad, M.R. & Manaf, A.A., 2011. Response estimation of micro-acoustic transducer for underwater applications using finite element method, *Indian Journal of Geo-Marine Sciences,* **40**, 176–180.

Zhang, K., Ju, X.D., Lu, J.Q. & Men, B.Y., 2014. Design of acoustic logging signal source of imitation based on field programmable gate array, *Journal of Geophysics and Engineering,* **11**, 045008.

Zhang, K., Ju, X.D., Lu, J.Q. & Men, B.Y., 2016. A debugging system for azimuthally acoustic logging tools based on modular and hierarchical design ideas, *Journal of Geophysics and Engineering,* **13**, 430.

Zhang, K., Ju, X.D., Tan, B.H., Lu, J.Q., Men, B.Y., Wu, W.H. & Chen, J.Y., 2017a. New excitation method for acoustic logging transmitters, *Journal of Geophysics and Engineering,* **14**, 751–757.

Zhang, K., Tan, B. & Liu, X., 2017b. A consistency evaluation and calibration method for piezoelectric transmitters, *Sensors,* **17**, 985.

Zhang, K. et al., 2021. Design of a new acoustic logging while drilling tool, *Sensors,* **21**, 4385.